Application of a Spectroscopic Infrared Focal Plane Array Sensor for On-Line Identification of Plastic Waste

W. H. A. M. van den BROEK, D. WIENKE, W. J. MELSSEN, R. FELDHOFF, T. HUTH-FEHRE, T. KANTIMM, and L. M. C. BUYDENS*

Catholic University of Nijmegen, Laboratory for Analytical Chemistry, Nijmegen, Toernooiveld 1, 6525 ED Nijmegen, The Netherlands (W.H.A.M.V.B., D.W., L.M.C.B); and Institute for Biochemical Sensor Research Münster, Wilhelm-Klemm-Str. 8, 48149 Münster, Germany (R.F., T.H.-F., T.K.)

A spectroscopic near-infrared imaging system, using a focal plane array (FPA) detector, is presented for remote and on-line measurements on a macroscopic scale. On-line spectroscopic imaging requires high-speed sensors and short image processing steps. Therefore, the use of a focal plane array detector in combination with fast chemometric software is investigated. As these new spectroscopic imaging systems generate so much data, multivariate statistical techniques are needed to extract the important information from the multidimensional spectroscopic images. These techniques include principal component analysis (PCA) and linear discriminant analysis (LDA) for supervised classification of spectroscopic image data. Supervised classification is a tedious task in spectroscopic imaging, but a procedure is presented to facilitate this task and to provide more insight into and control over the composition of the datasets. The identification system is constructed, implemented, and tested for a real-world application of plastic identification in municipal solid waste.

Index Headings: **Spectroscopic infrared imaging; Plastic identification; Focal plane array (FPA) detector; Linear discriminant analysis (LDA).**

INTRODUCTION

Near-infrared (NIR) spectroscopy is a well-known and accepted identification technique which finds its merits in agricultural science, pharmaceutical science, and process control.[1–3] A few years ago, as an extension of this technique, spectroscopic NIR imaging was introduced as a technique which generates additional identification information.[4–6] This method opens new doors, in particular, for process control and process monitoring. Identification by artificial vision provides additional geometric material information, which allows surface mapping of physicochemical properties. Furthermore, the shape and size of the samples can be used as additional sorting criteria, whereas the technique is independent of the position of the process (sample) in the measurement detection area. The latter is an important practical advantage. A main problem in spectroscopic imaging is the amount of data that is generated.[7,8] New IR imaging detectors, called focal plane array (FPA) or staring array detectors, combined with fast wavelength selection devices, allow the acquisition of millions of reflectance units. In order to extract the most relevant information from these data, fast electronics and computer algorithms combined with a thorough knowledge of the problem are needed. Earlier experimentation in unsupervised classification by the present authors[9,10] has now lead to the introduction of supervised multivariate statistical pattern recognition for on-line classification of large amounts of spectroscopic image data. The extraction of the relevant spectroscopic material information is done with linear discriminant analysis, which is a fast, robust, well-known, and frequently validated classification technique.[11] Supervised classification gives the opportunity to include pre-information in the classification model, which can improve the classification performance. So far, this approach has appeared to be a very time-consuming step for spectroscopic image data. While NIR spectroscopic imaging has already been applied in many microscopic applications,[12–17] developments in the macroscopic field have not been as rapid, and the applicability of chemometric techniques in this field has hardly been investigated. Therefore, the purpose of this paper is to investigate the merits of a macroscopic NIR imaging system suitable for on-line measurements. In this paper, an identification system for plastic waste identification is developed.

It has been known for some time that the direct recycling of unsorted plastic waste is of limited applicability for reuse in the industry, because of the poor physical and chemical properties of mixed plastics.[18] Therefore, this kind of waste needs to be sorted prior to further processing. Over the last few years, extensive growth in research has been observed for automated plastic waste identification techniques.[19–23] Several research groups have come to the conclusion that NIR spectroscopy is presently one of the most promising techniques. They have concluded that this technique is fast and accurate, does not need any contact (nondestructive), and does not require sample pretreatment. Detectors for the NIR wavelength region are relatively cheap and commercially available. The material recognition is based on interactions of light with vibrations of specific molecules which are present in polymers. This work aims at the detection of plastics from nonplastics in a stream of mixed waste by spectroscopic NIR imaging.[24] It is done within the EC project SIRIUS, a cooperation project between the Laboratory for Analytical Chemistry, University of Nijmegen, The Netherlands, and the Institute for Chemical and Biochemical Sensor Research, Münster, Germany. Another part of the project is to investigate the succeeding steps in plastic identification—namely, to separate out the different types of plastics from each other. A good discussion about this subject and the results of that work is presented in detail in the literature.[10,19,25,26]

In the first part of the present study, a description of the detection technique is given in order to show the large

Received 10 June 1996; accepted 18 November 1996.
* Author to whom correspondence should be sent.

0003-7028/97/5106-0856$2.00/0

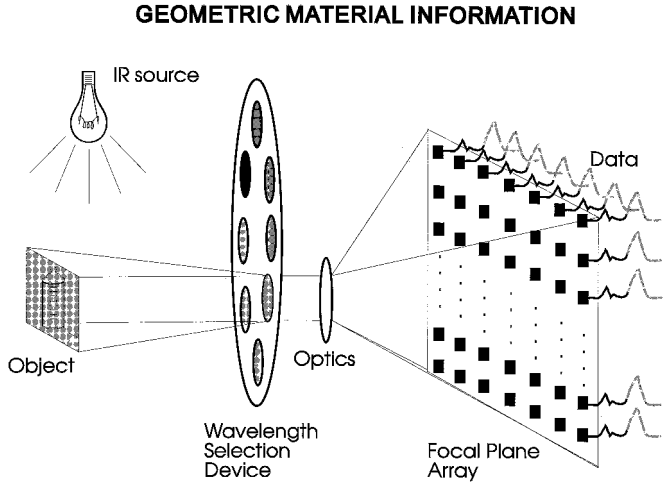

FIG. 1. Schematic view of the measurement principles. Reflected radiation from an object is measured for several wavelength regions. Each individual detector pixel integrates possible reflected photons in the particular wavelength range.

amount of data that is generated. Linear discriminant analysis (LDA) was used to extract material information from these data to determine the class membership of the measured object(s). The importance of supervised classification using a representative calibration model and test set is discussed, and an easy way to compose these sets for three-dimensional image data is given. A specific imaging filter was used to incorporate additional geometric material correlations in the image data. A special section is devoted to specific problems that occur in macroscopic imaging: shadow effects of large objects and mirror reflections due to the smoothness of an object's surface. Speed measurements were performed to investigate the future applicability of the setup and to compare the data-reducing classification technique with classification of the untreated, original image data. Finally, on-line measured images were classified by the optimized experimental setup and the optimized LDA model.

BACKGROUND

Spectroscopic Imaging. Spectroscopic imaging is based on the same principles as NIR transmission or reflectance spectroscopy. Most work has been presented as either microscopic applications where transmission measurements of the investigated materials were obtained or as large-distance applications such as satellite measurements. For the macroscopic experimental setup presented in this work, however, reflection measurements were used. In reflection measurements, the waste materials are illuminated by an infrared light source. The reflected light is passed through a wavelength selection device, as is shown in Fig. 1. In this figure a rotating filter wheel containing interference filters is used as a wavelength selection device. After passing this device, the reflected and filtered light is projected on the detector by an optical lens system. A new focal plane array detector is used, which contains thousands of sensing elements, pixels, which can individually integrate infrared photons over a wavelength range from 1200 to 4600 nm. A wavelength integration for one filter results in an image where every

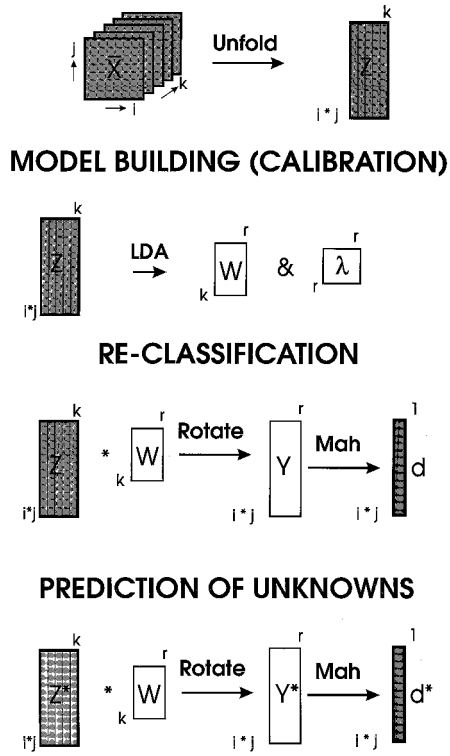

FIG. 2. Schematic representation of the LDA classification procedure. The three-dimensional calibration dataset $\bar{\mathbf{X}}$ is unfolded to a two-dimensional matrix **Z**, which is used to calculate weight matrix **W**. Next, matrix **Z** is transformed to **Y** where for each class (*nc*) the covariance matrix and corresponding means are calculated, according to the Mahalanobis measure. An unknown image **Z*** is transformed to **Y*** and classified to **d*** with the use of the calculated covariance and mean data.

element represents the total integrated value (gray value) for all reflected photons, collected from the corresponding geometric area. A measurement with different interference filters results in a three-dimensional stack of images, $\bar{\mathbf{X}}_{i,j,k}$, where the variables i and j are image coordinates, with $i = 1 \ldots n$, and $j = 1 \ldots m$, and where k represents the selected wavelength regions, with $k = 1 \ldots p$. Another representation of this three-dimensional stack is to consider every individual pixel as an independent detector, able to integrate reflected photons from a specific area in the camera view. Measuring images at p different wavelengths results in a matrix of vectors, were every p-dimensional vector expresses a so-called mini-spectrum. A p-dimensional vector is not a real spectrum, because the filter ranges are not successive, but this method of representation facilitates interpretation (also see next section).

Classification of Spectroscopic Image Data. A mini-spectrum can be considered as a vector in a p-dimensional wavelength space ($p = 6$ in this work). As every detector element is able to measure a mini-spectrum from a specific area (x,y) in the camera view, physicochemical information is obtained per corresponding (x,y) position and stored in $\bar{\mathbf{X}}_{i,j,k}$ (Fig. 2). Since equivalent materials express equivalent physicochemical properties, they are expected to express similar mini-spectra. Therefore, these mini-spectra can be used by pattern recognition techniques for classification, which leads to a complete mapping of the (x,y) positions in the camera view. The result

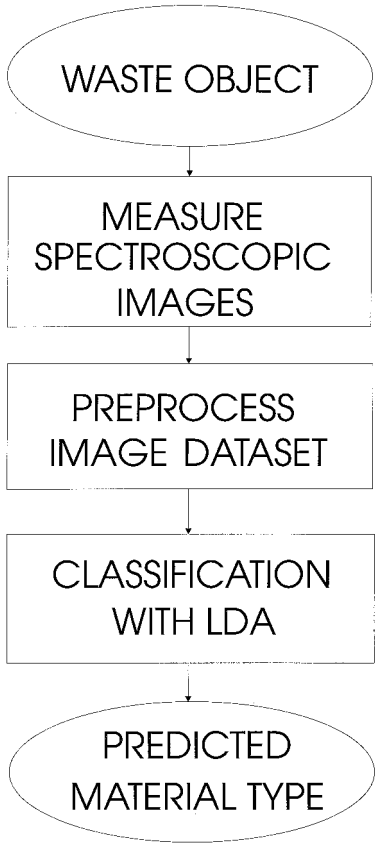

FIG. 3. Schematic representation of the on-line identification of plastic materials.

is stored in a matrix $\mathbf{D}_{i,j}$ where each element represents the class membership of the corresponding (x,y) positions. When the pattern recognition technique "classifier" is first calibrated (trained) with known mini-spectra, it can evolve a model which can be used to predict the class membership (material type) of unknown mini-spectra. First, a classification model is built by training the classifier with representative examples of the classes to be investigated. Second, when a robust model has been built, it can be used to predict the class membership of unknown samples. In this work, linear discriminant analysis is used as a pattern recognition technique. It is a known technique in chemical image analysis.[24] LDA tries to find the discrimination lines between classes of interest and uses these to estimate the most probable class membership of unknown samples, on the basis of the spectral information used for building the classification model. Figure 3 shows a summary of the different steps in the identification process.

EXPERIMENTAL

Hardware. Spectroscopic imaging was done with the experimental setup shown in Fig. 1. Four strong, variable, quartz light sources (1800 W each) were used to illuminate the objects, which were placed on the measurement area. This area was a sanded aluminum plate to establish diffusely reflected background radiation. A high illumination power was needed because of the large distance between object and detector, which was about 1.5 m. The light sources were positioned above the objects and in opposite directions in order to reduce shadow contributions around the objects. The angle of the light source and the plane perpendicular to the measurement area was about 67°. The reflected radiation from the objects was collected by a gold mirror and passed through a circular rotation filter wheel. This wavelength selection device contained $p = 6$ interference filters, which were transparent at, respectively, 1546–1578, 1545–1655, 1655–1745, 1700–2150, 2207–2321, and 2115–2550 nm. The filters are optimized for those specific wavelength regions that give maximum discrimination between plastics and nonplastics.[27] Thereafter, the photons were projected on the FPA detector (Cincinnati Electronics Inc., OH) by an ordinary 50-mm objective lens, $f = 1/2.3$. The objective lens material was transparent from 300 to 2700 nm.† As chromatic aberration of the ordinary objective lens caused different focus centers for different interference filters, two additional lenses were mounted on the filter wheel to correct for this artifact. These lenses were commercial silica lenses for filters 5 and 6, with focal lengths of, respectively, 4 and 2 m. In front of the detector, inside the camera, a cold-shield filter is positioned to prevent the detector from sensing background light emitted by the optical components. This cold-shield filter is cooled with N_2. The wavelength range of the cold-shield filter has been extended to 1.1–4.6 μm. The FPA detector was made of InSb and is sensitive from 1200 to 4600 nm. It contains 64×64 sensing elements (image size $n \times m$). The gray-scale resolution of the camera is 10 bits. The digital output of the camera was able to send 51 frames (images) per second via an electronic buffer (SC-01) and a high-speed 16-bit S16D I/O interface (Engineering Design Team, Inc. OR) to the internal memory of a SUN SPARC 10 workstation. Because of this construction, the images were available for image processing at approximately the camera readout speed.

Software and Computations. Direct image access was established by a library of C procedures, developed and installed by Starling Consultancy (Hengelo, The Netherlands). This library is used to process and classify the raw images by self-implemented procedures. The classification models were made by another program beforehand with the use of MATLAB (The MathWorks, Inc., Natick, MA). MATLAB has also been used for visualization and other calculations. The preparation of the training and test datasets was performed by an in-house-developed score plot program. This program used XITE software procedures (Torr Lonnestad and Otto Milvang, Image Processing Laboratory, Department of Informatics, University of Oslo, Norway) for graphical display of the score plots and mouse interactions.

MATERIALS AND METHODS

Dataset. Objects or samples with known material composition are needed in order to calibrate (learn) the material properties by LDA. In this work, it is supposed that spectroscopic NIR images, measured from such samples, contain sufficient information to discriminate between the materials. As a consequence, a number of waste samples

† Measurements taken from different objective lenses, performed by H.W. Siesler and students, NIR research group, University of Essen, Germany.

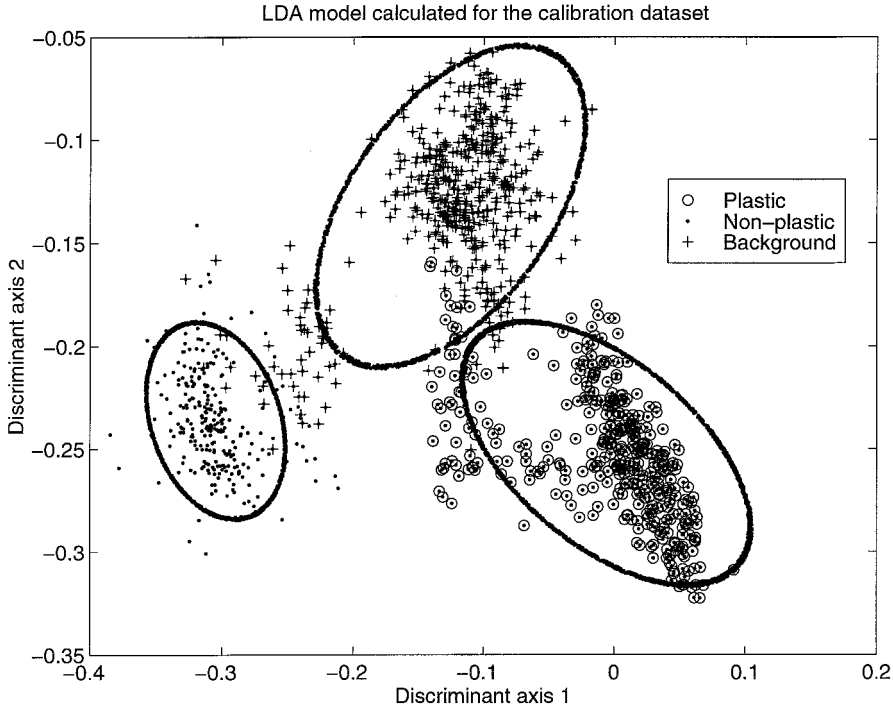

FIG. 4. Visualization of the calibration dataset using two linear discriminant components for three classes: plastic, nonplastic, and background mini-spectra. The ellipses indicate the classes modeled by LDA.

were collected from the household waste of the city of Nijmegen (The Netherlands).

In total, 40 waste objects were collected comprising 17 plastics [1 PVC (polyvinylchloride), 2 PET (polyethyleneterephthalate), 4 PS (polystyrene), 4 PE (polyethylene), and 6 PP (polypropylene)] and 23 nonplastics (4 ceramics, 5 metals, 3 glass, 5 paper, 5 wood, and 1 fiber). The objects differed in size, color, composition, mechanical flexibility, and thickness. Images were measured by using six interference filters per object and corrected for the dark current and reference images as described in the literature.[25] This correction entails the division of the raw image by its corresponding reference image. The resulting corrected image sets the reflectance values for dead pixels to 1. Since this is equal to the scaled background value in the corrected image, the dead pixels did not need any further processing for the purpose in this work. After preprocessing, 40 stacks of corrected images ($64 \times 64 \times 6$) were obtained and stored as a database. The database was used to create a training and test set. The training set was used to build the model by the pattern recognition technique and the test set to evaluate the calculated model.

Training and Test Set. A complete three-dimensional stack of images (size: $n = 64$, $m = 64$, $p = 6$) contains only information from a single (waste) object. Since each stack of images contains 64×64 pixels, representing 4096 mini-spectra each of length $p = 6$, a huge amount of data is obtained for only one material sample. To include sufficient variation in material type for both the calibration and test set, one needs to characterize many material samples by their image stacks. Therefore, a compromise has to be found between a representative variation in material type and the total size of training and test dataset. To solve this, we created a training and test dataset, by extracting a predefined number of material pixels (plastic or nonplastic) and background pixels from a series of image stacks. The numbers were chosen in such a way that the calibration dataset contained about the same number for each material class. Two ways of selecting these pixels from the images were investigated. The first was by visual inspection of the images, the second by means of principal component analysis (PCA).[25]

By visual inspection, fixed blocks of pixels were extracted from "pure" material areas in the image. Care had to be taken to exclude pixels with bad mini-spectra such as mirror reflection or spikes. A problem with visual inspection is that large-sized blocks do not guarantee homogeneous material information, whereas small blocks lead to very time-consuming pixel extraction. Pixel selection by principal component analysis guarantees the selected homogeneity of the mini-spectra and is very easy to perform. The PCA selection is based on the spectral correlation of pixels in a score plot. A cluster in a score plot can be selected by mouse-assisted handling on a computer screen. Since there is little control about the number of pixels in a selected cluster of a PCA score plot, it is necessary to reduce the amount of selected pixels to a predefined number. This selection is done randomly.

The training set was created by selecting an equal number of pixels for each material, but it should be stressed that the nonplastic class consisted of six materials instead of five for the plastic class. Pixels from the remaining materials were all put into the test set. Since a different number of objects per material were collected, a different number of pixels are present in the test set.

The final numbers of pixels in the calibration set were as follows: plastics, 400; nonplastics, 450; and background, 400. For the test set, the numbers were as fol-

TABLE I. α ("false negative"), β ("false positive"), and total error in percentages and number of pixels, respectively, calculated for the test set. Three different scaling techniques were applied for the three-class model, while the four-class dataset is the extended three-class dataset including shadow pixels.

	Comparison of classification errors				
	3-class	3-class unit	3-class range	3-class auto	4-class
$\alpha_{plastics}$	2.00 (9)	12.0 (54)	0.44 (2)	0.67 (3)	0.22 (1)
$\alpha_{nonplastics}$	5.57 (39)	2.43 (17)	5.29 (37)	5.00 (35)	12.6 (88)
$\alpha_{background}$	0.17 (1)	68.0 (410)	10.8 (65)	1.00 (6)	1.17 (7)
$\beta_{plastics}$	2.08 (27)	1.31 (17)	2.85 (37)	2.46 (32)	2.00 (26)
$\beta_{nonplastics}$	0.95 (10)	44.2 (464)	6.38 (67)	0.86 (9)	0.48 (5)
$\beta_{background}$	1.04 (12)	0.0 (—)	0.0 (—)	0.26 (3)	0.35 (4)
Total %	2.80 (49)	27.5 (481)	5.94 (94)	2.51 (44)	5.49 (96)

lows: plastics, 450; nonplastics, 700; and background, 600.

LDA Methodology. The identification problem in this work is to classify image pixels into the three aforementioned material classes: plastic, nonplastic, and background. These classes need to be modeled before pixel classification of unknown material pixels can take place. The multiple class modeling will be done by linear discriminant analysis. A detailed description of LDA can be found in the literature.[28] The final classification of unknown mini-spectra is performed by determining the shortest Mahalanobis distance (D^2) between the unknown and the existing material classes. The Mahalanobis distance of object i to class c is defined as $D^2_{i,c} = (\mathbf{x}_{i,c} - \mathbf{xm}_c)' \mathbf{S}_c^{-1} (\mathbf{x}_{i,c} - \mathbf{xm}_c)$,[29] where $\mathbf{S}_c^{-1}$ represents the inverse of the covariance matrix of class c, $\mathbf{xm}_c$ is the mean or centroid of class c, and $\mathbf{x}_{i,c}$ represents the mini-spectrum from object i, belonging to class c. In this way, correlation or covariances in the material classes are taken into account explicitly.

The LDA model consists of (r) discriminant weights, where r represents the number of linear components. Each weight is a linear combination of the original wavelength regions. The discriminant weights are used to transform original unknown mini-spectra (pixels) to the latent model space. Subsequently, the Mahalanobis distances are calculated between the unknown image pixels and each individual class center within this new reduced space (centroid). The unknown pixel is classified to the class where the Mahalanobis distance between pixel and class centroid is the shortest. An example of the LDA model with Mahalanobis classification is shown in Fig. 2. First, the LDA model is calculated by using the calibration mini-spectra in the unfolded matrix $\mathbf{Z}_{n*m,p}$. The folding of images has been described earlier.[25] The model leads to a weight matrix $\mathbf{W}_{p,r}$ and their corresponding column importances $\lambda_{r,r}$. The weight matrix $\mathbf{W}_{p,r}$ can then be used to reduce the $\mathbf{Z}_{n*m,p}$ matrix to the discriminant space, represented by $\mathbf{Y}_{n*m,r}$. From these transformed training pixels the class centroids $\bar{\mathbf{Z}}_c$ and corresponding covariance matrices $\mathbf{C}_c$ of each class c are calculated. In the same way, unknown mini-spectra in the test matrix $\mathbf{Z}^*_{n*m,p}$ can be transformed to their discriminant space $\mathbf{Y}^*_{n*m,r}$. Their class membership can be predicted by the Mahalanobis distances by using $\bar{\mathbf{Z}}_c$ and $\mathbf{C}_c$. The classification result is expressed by the vector $\mathbf{d}_{n*m}$, in which integer-valued elements represent the membership of each image pixel in a particular material class. It should be noted that the maximal dimension of r is defined as: $r = \min(p, nc - 1)$, where nc is the number of classes. The vector $\mathbf{d}_{n*m}$ can be folded back to an image $\mathbf{D}_{n,m}$, which facilitates a direct evaluation by means of visual inspection.

Filtering of Classified Images. Another important inherent characteristic of multivariate images is the high correlation between adjacent pixels. In the classification process, only the spectral information is used. In order to use the additional geometric correlation, a filtering procedure was applied to the images. This filter, referred to as a majority filter, checks for the class membership of the neighbor pixels. The class membership of the pixel under investigation is replaced by that of the majority of the neighboring pixels. This is done by first defining a window around the pixel to be examined. This window has a size of $s*s$ where s must be uneven. When a predefined number of neighbors m, where m is larger than $0.5*(s*s - 1)$, have the same class membership as the central pixel, then the class membership of the central pixel is replaced by that of the majority. The decision about the number of pixels within the window that should represent the majority is dependent on the size of the window and is problem-specific. In this work, the classified images have been filtered by using a window size of 3*3 with a majority threshold of 6. In this way, the high correlation between neighboring pixels is taken into account. As most waste objects are positioned around the image center, the edges of the images are not filtered.

RESULTS AND DISCUSSION

Inspection of Calibration Dataset. Figure 4 shows the mini-spectra (pixels) from the calibration dataset, plotted for the first two discriminant axes of the LDA model. As mentioned previously, the maximum number of discriminant weights (r) that can be calculated is defined by $r = \min(p, nc - 1)$, where $p = 6$ (the number of interference filters) and $nc = 3$ (the number of classes). This means that there are maximally two discriminant weights which can be calculated for these data. The plot shows that the information content in the mini-spectra allows a discrimination between the three material classes: plastic, nonplastic, and background. There is a small overlap for nonplastic and background pixels. It turned out that the overlapping pixels were selected from transparent glass. Obviously, the small absorbance of this glass is hard to detect by our experimental setup within the wavelength regions used. This consideration makes it difficult to discriminate the

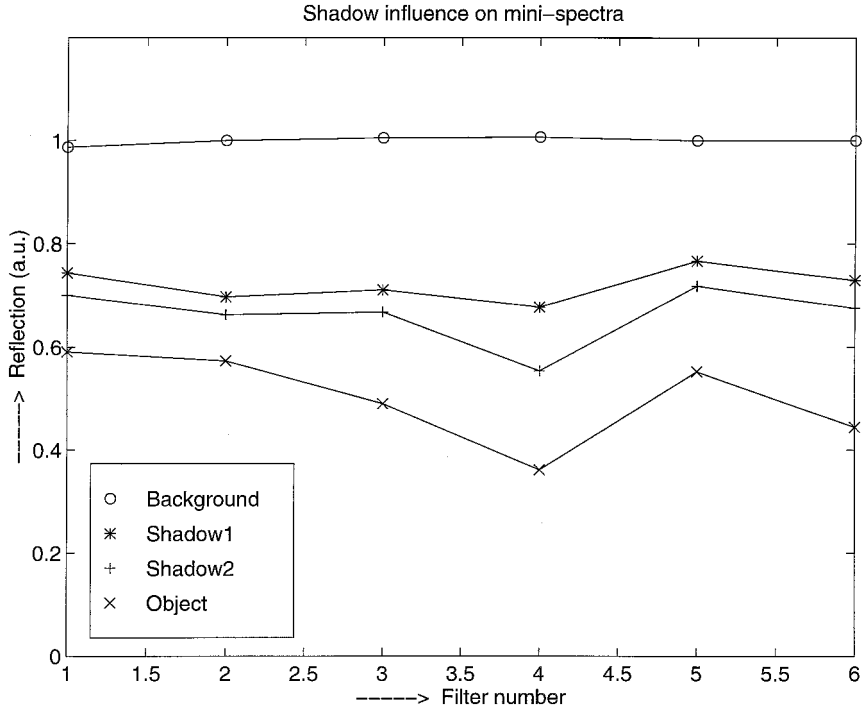

FIG. 5. Influence of shadow on mini-spectra. The mini-spectra shown are taken from the indicated positions in Fig. 6B. The mini-spectrum for background material shows no spectral features, but the two shadow spectra resemble the mini-spectrum for the nonplastic material.

glass from the background material. Another overlap exists between plastic and nonplastic materials. This overlap was due to thin and transparent plastic foils whose mini-spectra did not clearly exhibit the features of one of the plastic spectra. The three ellipses in the plot indicate equidistant distances from each corresponding class center, with the use of the Mahalanobis distance measure. As this measure takes the cluster variance into account, the ellipse of a compact cluster (small standard deviation) will enclose a smaller area than a cluster which is more diffuse (large standard deviation). The ellipses are calculated by multiplying the class standard deviations with the same (arbitrary) number. Because the spread in the cluster for background pixels (for both axis) is the smallest, the corresponding ellipse is also the smallest. Note that the plot shows regions of extrapolation (empty areas within the ellipse) for both plastic and nonplastic materials.

Test Set Classification. The prediction ability of the LDA model is validated with the test set. The classification results for the test set are shown in Table I. We tried to improve the classification results by preprocessing the data prior to calculating the model. Therefore, several scaling techniques were applied on the corresponding mini-spectra. To compare the influence of the different scaling techniques, we formulated a zero-hypothesis (Ho) for each material type:

> Ho: The classification result is material *c* if the Mahalanobis distance of this object pixel in the transformed LDA space to the centroid of class *c* is the smallest, where *c* can be one of the material classes—plastic, nonplastic or background.

The α error is defined as the rejection of Ho while it is true ("false negative"). The β error is defined as the acceptance of Ho while it is false ("false positive"). It cannot be predicted which of these errors is important and what their values should be. This factor depends on the desired sorting criteria. When a high material purity is required, the β error must be as small as possible. This means that the percentage of other materials in the (already) sorted plastic waste is kept to a minimum. For example, when the β error for material class *c* is zero, all samples in the test dataset which do not belong to class *c* are not classified as being material class *c*. On the other hand, when a high yield of sorted material is required, the α error should be as low as possible. For example, when the α error for material class *c* is zero, all the corresponding samples in the test dataset belonging to class *c* are classified correctly. In plastic recycling, the β error is an important purity parameter, since different types of plastic do not mix well and only very pure mono-streams can be processed to high-value products. In this case, a very low β error is required. One should keep in mind that a low β error can result in a low yield since only the very pure materials are extracted from the waste. On the other hand, when the recycled plastic material is destined for low-value products, the yield is very

TABLE II. Time calculations for hardware and software in ms. The hardware measurements were executed in a stand-alone mode, without the use of the filter wheel, but include the correction of the images for background and dark current contributions.

		With LDA (ms)	Without LDA (ms)
Hardware:	Measurements	631	631
Software:	Step 1	30	—
	Step 2	284	829
	Step 3	63	63
	Total	377	892

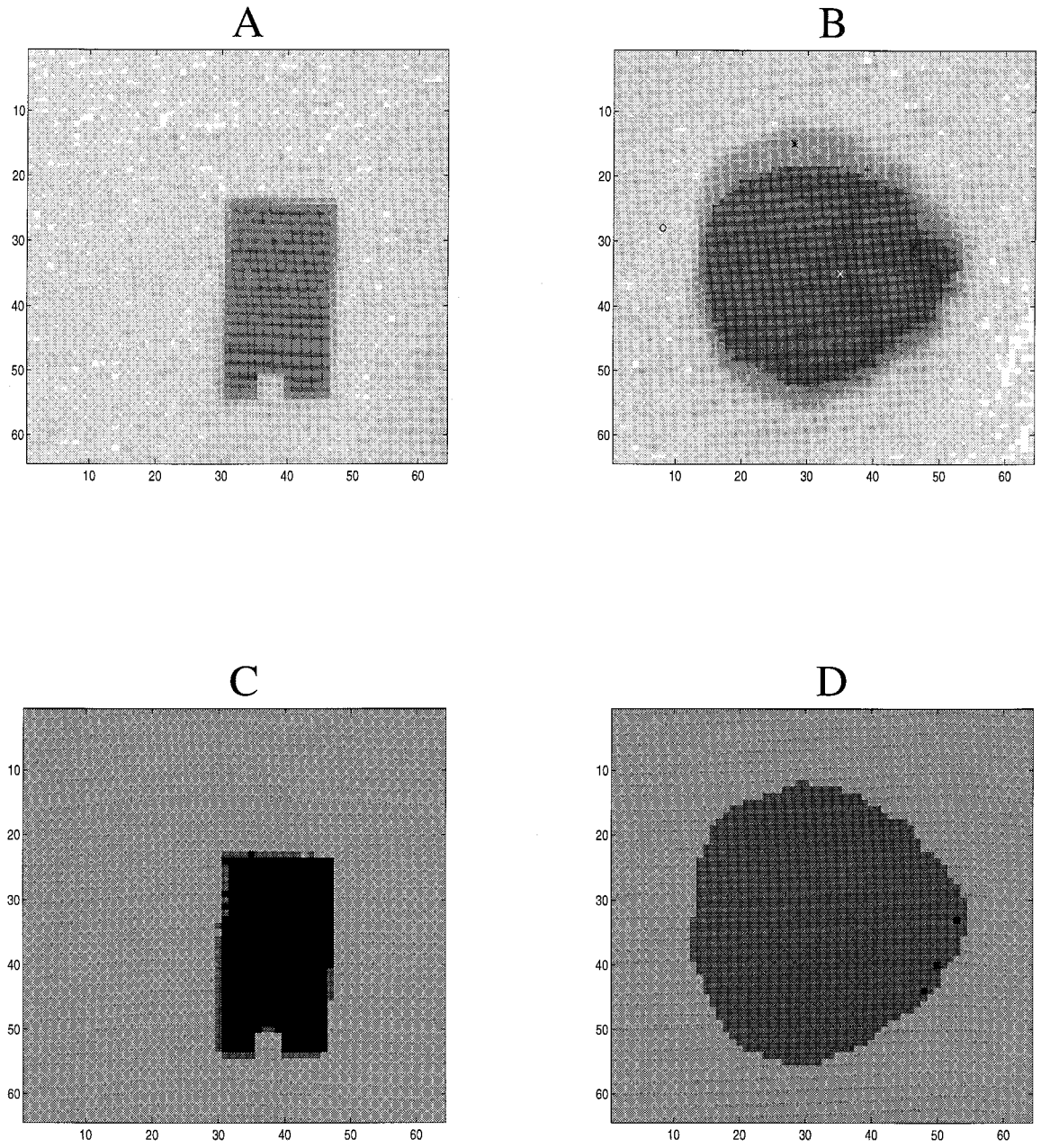

FIG. 6. (**A** and **B**) Example of two original raw images, measured from a plastic (PET) fragment and a cotton sock, in the spectral range from 2100 to 2500 nm. Note the shadow regions for the cotton sock. (**C** and **D**) The raw images from **A** and **B** are classified by the three-class LDA model. Black represents plastic material, light gray the background, and medium gray the nonplastic material. Shadow and edge effects are not recognized by the model. (**E** and **F**) The raw images from **A** and **B** are classified by the four-class LDA model. Shadow and edge effects are partly recognized by the model. (**G** and **H**) The raw images from **A** and **B** are classified by the four-class LDA model and filtered with the majority filter. Shadow and background classes are represented by the light gray color as one class.

important and should be very high. This standard can be achieved by a low α error. It depends on the quality demands of the low-value product to what extent the β error may occur.

Three different scaling techniques were applied on the three-class model: unit length, range (0–1), and autoscaling. The four-class dataset is the extended three-class dataset including shadow pixels. The α and β classification errors were calculated for each material class.

The best classification results are obtained when autoscaled mini-spectra are used. Normalization to unit length and range scaling between 0 and 1 yielded bad classification results, while mean centering gave exactly the same results achieved without preprocessing of the mini-spectra. As both the plastic and nonplastic samples are compiled from various materials, their corresponding mini-spectra express a large within-group variance. Since autoscaling takes this variance into account, it can lead to better classification results. Although the overall classification is just slightly better than classification of the untreated mini-spectra, we nevertheless decided to use the untreated mini-spectra for further classification. The reason for this decision was that scaling techniques require additional computation time, which reduces the speed for on-line measurements. This choice could be made because the classification performance without

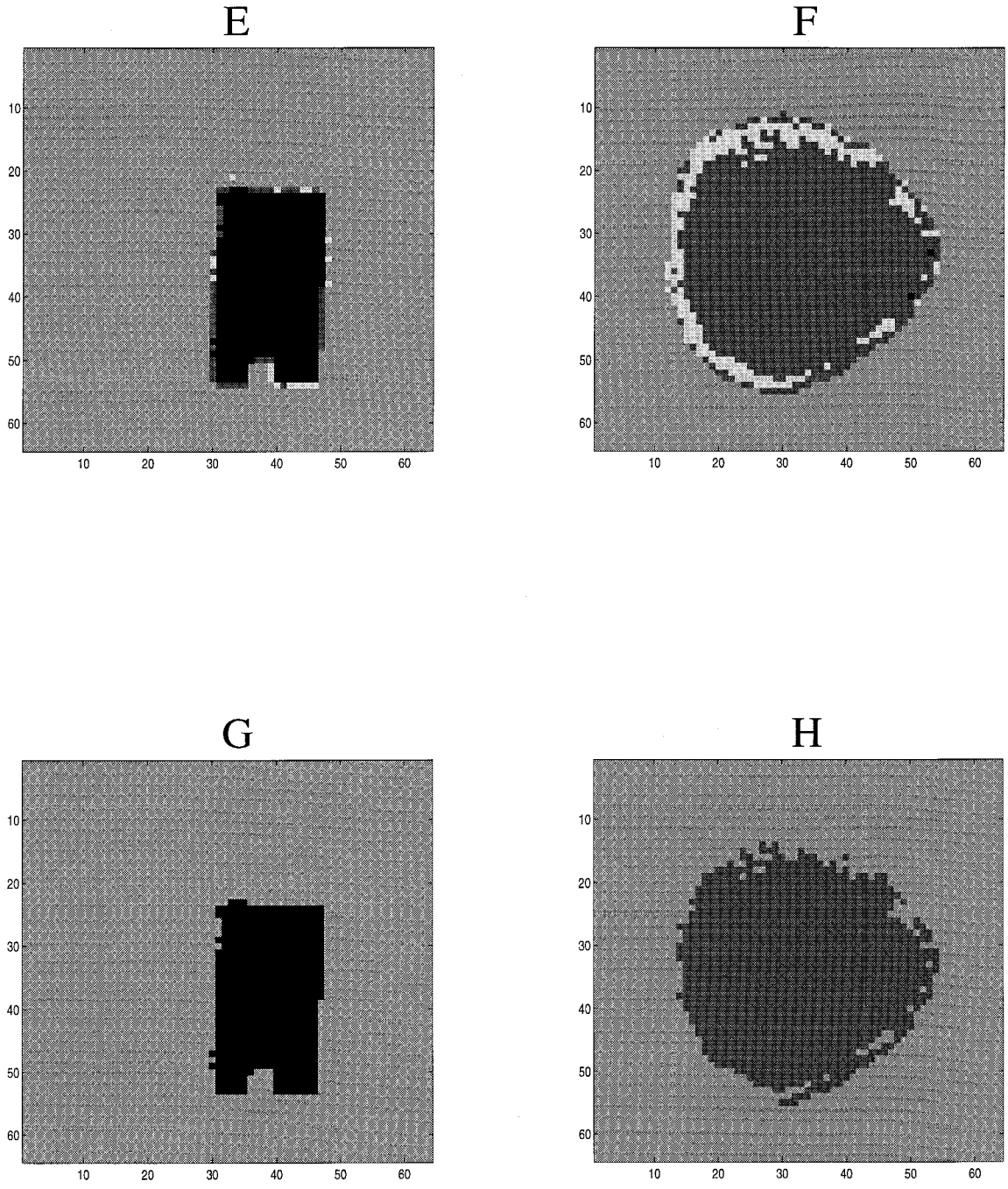

FIG. 6. Continued.

scaling was not significantly worse than that with scaling. An additional problem appeared when the three-class model was tested on real images. It turned out that small shadow bands around the objects were wrongly classified. This artifact was studied in more detail.

Influence of Shadow. In Fig. 5, a plot of four different mini-spectra is shown. These spectra were obtained from different areas in the image, as indicated by the corresponding symbols in Fig. 6B. The upper spectrum was measured from pure background material, whereas the lower spectrum originated from a nonplastic material. The remaining spectra were obtained from areas in the shadow region. Spectrum "Shadow1" was obtained from a region further away from the object sample than spectrum "Shadow2". From these spectra it can be seen why the shadow spectra differ from the object material spectra. The shadow spectra exhibit the same spectral structure as the object material, except for a constant difference (offset) in absorbance. The closer a shadow pixel is to the object, the smaller the offset difference in comparison with the spectrum of the object material. This offset difference must be caused by the lower intensity of the reflected radiation of these spatial regions, because shadow areas are less illuminated than others. The reason why shadow spectra resemble the spectra of the object has to do with the type of reflection. As diffuse reflected radiation leaves the object surface in all directions, a (small) part of this radiation can be captured by neigh-

boring pixels in the FPA detector and influence their spectra (also see next section).

On-Line Classification of Real Images. For on-line classification of raw images, two objects were chosen from two different materials—a nonplastic folded cotton sock and a plastic (PET) fragment. The raw images of these objects are depicted in Figs. 6A and 6B. Both images are easy to discriminate from the background, although it should be noted that the image measured from the sock contains shadow contributions on the upper and lower side of the sock. When the three-class LDA model was used to classify these raw images, it had difficulties in identifying the shadow contributions, because the model was not trained for this artifact (Figs. 6C and 6D). The edges of the plastic object were even recognized as nonplastic material. To overcome this problem in the short term, we added an extra shadow class to the LDA model. This class is identified as the four-class model. Additional shadow pixels (400) were extracted from stacks of images, measured from high objects. The selection of these pixels went through the same procedure as described before. Consequently, the LDA calibration model was extended to four classes. Table I shows that the classification results for plastics and especially for nonplastics became a little bit worse. The extra class forced the LDA model to include it in the old model, resulting in a loss of discrimination power for the existing classes. Since the shadow spectra resembled those of the nonplastic, the discrimination between these spectra is more difficult. The two models show that a choice has to be made when raw images are to be classified. The three-class model predicts the three material types better than the four-class model but cannot handle the image artifacts such as shadowed areas. To investigate the worst case, we depict the classification of the aforementioned raw images performed with the four-class model in Figs. 6E and 6F. Although some false classifications occurred near the edge of the object, the four-class model was for the most part capable of recognizing large areas of shadow around the object. After including the geometric correlation in the images by the majority filter and representing the background and shadow class by one combined class (see Figs. 6G and 6H), we could easily recognize the material class of the measured objects.

Speed Measurements. One of the requirements for on-line identification is fast image processing. Therefore, speed measurements for the individual hardware and software components have been carried out, ranging from the image measurement step to the classification of the image pixels for a complete stack of images. The slowest step of the present experimental laboratory setup is due to the slow communication between computer and rotating filter wheel. This delay in the procedure of setup reduced the measurement time for one identification to about 6 s. Because of this consideration, the speed measurements are calculated per individual step, to estimate the decision speed of the experimental setup, when the communication problem of the filter wheel is solved. In Table II, a time table is given for the individual steps. The LDA classification is compared with classification of the unreduced original mini-spectra, with the use of only the Mahalanobis distance measure. The table shows that the measurement time for the software processing part is much shorter than that for the hardware, if LDA is used for classification. The software computation time comprises three substeps. In step 1, the raw mini-spectra have to be transformed to the discriminant space (only for LDA classification). Step 2 comprises the calculation of Mahalanobis distances from the transformed mini-spectra to all class centroids. In the last step, the shortest class distance for each mini-spectrum is calculated and all classified mini-spectra are counted. When the time consumption of LDA classification is compared with that for classification of the original, unreduced mini-spectra, a time reduction of a factor 2.4 is obtained. Although LDA classification needs an extra transformation step (step 1), more time is gained with the distance calculations. This gain will even increase when more interference filters are used, since more operations are needed in the distance calculations of step 2!

Future Expectations. The use of the present experimental setup for the identification of different types of plastics is presently under investigation. For this goal to be accomplished, either more wavelength regions have to be taken into account (requiring the installation of more interference filters) or smaller filter widths have to be used. Both options are meant to measure more specific information from the waste materials, since the spectra of, e.g., PE and PP show only small differences within a limited wavelength range.[19] Furthermore, for the application of such a system in practice, it should have no moving parts as well as high measurement and classification speed.

To guarantee fast, safe, and robust classification of spectroscopic image data, future research will focus on the implementation of other multivariate identification techniques such as artificial neural networks and a bootstrap-based classification technique[30] with error indication. Preliminary results of artificial neural networks as advanced, nonlinear, multivariate classification methods, applied to spectroscopic imaging, have already been presented.[31]

CONCLUSION

In the present work we have demonstrated that spectroscopic near-infrared imaging can be used for rapid on-line material identification on a macroscopic scale. An important requirement is that multivariate statistical identification techniques be used, which reduce the large amount of spectroscopic image data for faster data handling. The classification results showed that an empirical pattern recognition technique, such as LDA, is very suitable for the on-line classification of spectroscopic images. This technique is fast and robust and reduces the large stacks of image data. The necessity of preparing a calibration and test dataset also accounts for spectroscopic image data; accordingly, an easy way of performing this procedure by means of principal component analysis is presented. This procedure facilitates the access for other spectroscopic imaging techniques to identify materials on the basis of their differences in physicochemical properties. The present experimental laboratory setup is able to measure sufficient information from the waste materials to discriminate between them. The recognition percentage for plastics and nonplastic materials by LDA is high-

er than 97%. This level is significantly better than that achieved with the recently reported unsupervised classifier.[10] Nevertheless the on-line classification of complete images showed additional practical problems such as the influence of shadow and speed contributions.

ACKNOWLEDGMENTS

The authors gratefully acknowledge financial support from the Commission of European Communities for awarding Environmental Grant No. EVWA-CT-92-0001. Thanks also go to K. de Crom and A. Kraak for measurement and processing of the image dataset, E.W. van de Ven for help in building classification models and writing the identification software, and L. ten Horn and R. Gelsing for installation of the rotating filter wheel.

1. H. W. Siesler, NIR News, **6,** 3–12 (1995)
2. P. Williams and K. Norris, *Near Infrared Technology in the Agricultural and Food Industries* (American Association of Cereal Chemists, St. Paul, Minnesota, 1990), 2nd ed.
3. I. Murray and I. A. Cowe, in *Making Light Work: Advances in Near Infrared Spectroscopy,* Proceedings of the 4th International Conference on Near Infrared Spectroscopy (VCH Publishers, New York, 1992).
4. P. Geladi, S. Wold, and K. Esbensen, Anal. Chim. Acta **191,** 473 (1986).
5. W. F. McClure, NIR News **2,** 2, 8 (1991).
6. P. J. Treado and M. D. Morris, Appl. Spectrosc. Rev. **29,** 1 (1994).
7. B. Novales, D. Bertrand, M. F. Devaux, and P. Robert, "Assessment of the Quality of Wheat Milling Products by Fluorescence Video Imaging," International Conference on Quality Control by Artificial Vision, Le Creusot, France (1995).
8. E. N. Lewis and I. W. Levin, Appl. Spectrosc. **49,** 672 (1995).
9. D. Wienke, W. H. A. M. van den Broek, and L. M. C Buydens, Anal. Chem. **67,** 3760 (1995).
10. D. Wienke, W. van den Broek, W. Melssen, L. Buydens, R. Feldhoff, T. Huth-Fehre, T. Kantimm, F. Winter, and K. Cammann, Fresenius J. Anal. Chem. **354,** 823 (1996).
11. P. J. Treado and M. D. Morris, "Infrared and Raman Imaging", in *Microscopic and Spectroscopic Imaging of the Chemical State,* M.D. Morris, Ed. (Marcel Dekker, New York, 1993), Vol. 16, pp. 3, 71–108.
12. M. Grassenbauer, G. Friedbacher, H. Hutter, and G. Stingeder, Fresenius J. Anal. Chem. **346,** 594 (1993).
13. M. A. Harthcock and C. Atkin, Appl. Spectrosc. **42,** 449 (1988).
14. E. N. Lewis and I. W. Levin, Vib. Spectrosc. Microsc. **1,** 35 (1995).
15. P. Geladi, J. Swerts, and F. Lindgren, Chemom. Intell. Lab. Syst. **24,** 145 (1994).
16. L. A. Cassis and R. A. Lodder, Anal. Chem. **65,** 1247 (1993).
17. H. Ritzmann and D. Schudel, Kunststoffe **84,** 582 (1994).
18. N. Eisenreich, 23rd International Annual Conference of ICT 1992: *Waste Management of Energetic Materials and Polymers,* Karlsruhe, Germany (1992), 59.1–59.12.
19. Th. Huth-Fehre, R. Feldhoff, Th. Kantimm, L. Quick, F. Winter, K. Camman, W. van den Broek, D. Wienke, W. Melssen, and L. Buydens, J. Mol. Structure **348,** 143 (1995).
20. M. K. Alam, S. L. Stanton, and G. A. Hebner, Spectroscopy **9,** 30 (1994).
21. D. M. Scott and R. L. Waterland, Polym. Eng. Sci. **35,** 1011 (1995).
22. H. Ritzmann and D. Schudel, Kunstoffe **84,** 582 (1994).
23. D. Wienke, W. van den Broek, L. Buydens, T. Huth-Fehre, R. Feldhoff, T. Kantimm, and K. Cammann, Chemom. Intell. Lab. Syst. **32,** 165 (1996).
24. P. Robert, D. Bertrand, M. F. Devaux, and A. Sire, Anal. Chem. **64,** 664 (1992).
25. W. H. A. M. van den Broek, D. Wienke, W. J. Melssen, C. W. A. de Crom, and L. M. C Buydens, Anal. Chem. **67,** 3753 (1995).
26. R. Feldhoff, T. Huth-Fehre, T. Kantimm, L. Quick, K. Cammann, W. van den Broek, D. Wienke, and H. Fuchs, J. Near Infrared Spectrosc. **3,** 3 (1995).
27. W. H. A. M. van den Broek, D. Wienke, W. J. Melssen, and L. M. C. Buydens, paper accepted for publication in Appl. Spectrosc. (1997).
28. W. R. Dillon and M. Goldstein, *Multivariate Analysis: Methods and Applications,* (John Wiley and Sons, New York, 1984).
29. D. L. Massart, B. G. M. Vanderginste, S. N. Deming, Y. Michotte, and L. Kaufman, *Chemometrics: A Textbook* (Elsevier, Amsterdam, 1988), Vol. 2.
30. R. A. Lodder and G. M. Hieftje, Appl. Spectrosc. **42,** 1351 (1988).
31. W. H. A. M. van den Broek, NIR-95, The Future Waves, 7th International Conference on Near-Infrared Spectroscopy, Montreal, Canada (1995), Abstracts and Programs, 5.2.